Microchimica Acta (2021) 188: 358
https://doi.org/10.1007/s00604-021-05021-7

ORIGINAL PAPER

Simultaneous electrochemical determination of DNA nucleobases using AgNPs embedded covalent organic framework

P. Arul[1] · Sheng-Tung Huang[1] · N. S. K. Gowthaman[2] · Sekar Shankar[3]

Received: 26 April 2021 / Accepted: 7 September 2021 / Published online: 1 October 2021
© The Author(s), under exclusive licence to Springer-Verlag GmbH Austria, part of Springer Nature 2021

Abstract

An efficient electrochemical biosensor has been developed for the simultaneous evaluation of DNA bases using AgNPs-embedded covalent organic framework (COF). The COF (*p*-Phenylenediamine and terephthalaldehyde) was synthesized by reflux (DMF; 150 °C; 12 h) and the nanoparticles were embedded from the aqueous solutions of $AgNO_3$ and $NaBH_4$. The nanocomposite-modified COF was confirmed by spectral, microscopic, and electrochemical techniques. The nanocomposite material was deposited on a glassy carbon electrode (GCE) and the redox behavior of AgNPs was confirmed by cyclic voltammetry. The electrocatalytic activities of DNA bases were analyzed by differential pulse voltammetry (DPV) in a physiological environment (PBS; pH = 7.0) based on simple and easy-to-use electrocatalyst. The AgNPs-COF/GCE showed well-defined anodic peak currents for the bases guanine (+ 0.63 V vs. Ag/AgCl), adenine (+ 0.89 V vs. Ag/AgCl), thymine (+ 1.10 V vs. Ag/AgCl), and cytosine (+ 1.26 V vs. Ag/AgCl) in a mixture as well as individuals with respect to the conventional, COF, and AgNPs/GCEs. The AgNPs-COF/GCE showed linear concentration range of DNA bases from 0.2–1000 µM (guanine; (G)), 0.1–500 µM (adenine (A)), 0.25–250 µM (thymine (T)) and 0.15–500 µM (cytosine (C)) and LOD of 0.043, 0.056, 0.062, and 0.051 µM (S/N = 3), respectively. The developed sensor showed reasonable selectivity, reproducibility (RSD = 1.53 ± 0.04%–2.58 ± 0.02% (n = 3)), and stability (RSD = 1.22 ± 0.06%–2.15 ± 0.04%; n = 3) over 5 days of storage) for DNA bases. Finally, AgNPs-COF/GCE was used for the determination of DNA bases in human blood serum, urine and saliva samples with good recoveries (98.60–99.11%, 97.80–99.21%, and 98.69–99.74%, respectively).

Keywords Covalent organic framework · Silver nanoparticles · Differential pulse voltammetry · DNA bases · Biological fluids

Introduction

Deoxyribonucleic acid (DNA) plays an important role in the storage of genetic information, controls the synthesis of bioproteins and enzymes via the process of replication, and transcription of genetic information [1]. DNA bases are 3D biological network structures consisting of two distinct double helix chains [2]. The nucleobases are divided into two different complementary units namely purine-guanine (G), and adenine (A)), pyrimidine-thymine (T), and cytosine (C)) [1, 2]. The DNA bases can participate in a variety of cellular energy transductions through enzyme-based reactions [3]. Uncontrolled changes in purine and pyrimidine concentrations in biological living systems cause mutations in immunity, cancer, epilepsy, diseases with genetic predisposition, prostatitis, and Parkinson's disease [1, 3]. The presence of DNA bases in biologically important fluids could be the result of enzyme failure in tissue degradation or other metabolic mechanisms. Therefore, quantifiable measurements of DNA bases are needed from a clinical and biological perspective.

A number of analytical techniques exist for DNA bases, including chemical luminescence [4], Raman spectroscopy

✉ P. Arul
vpsarul@gmail.com; ws75624@ntut.edu.tw

✉ Sheng-Tung Huang

[1] Institute of Biochemical and Biomedical Engineering, Department of Chemical Engineering and Biotechnology, National Taipei University of Technology, Taipei, Taiwan, Republic of China

[2] School of Engineering, Monash University, 47500 Bandar Sunway, Malaysia

[3] School of Material Science and Engineering, Nanjing University of Science and Technology, Nanjing 210094, People's Republic of China

[5], spectrophotometer [6], HPLC [7], GC–MS [8], and capillary electrophoresis [9]. Most of these analytical techniques are well recognized but have some limitations. Researchers have attempted to develop electrochemical sensors for quantitative analysis of purine and pyrimidine nucleobases [10]. The electrochemical technique has a number of advantages [10–17]. Meanwhile, G and A are two important base pairs and active, the resolution of DNA bases is quantitative detection of G and A by electrochemical. Moreover, the current response of G and A at the unmodified surfaces has some remarkable difficulties such as broad oxidation peaks, poor electron transfer kinetics, extended background current, and more positive detection potential [15, 16]. To overcome the above shortcomings, the conventional electrode surface was modified with electroactive materials, and then used for sensitive and selective determination of DNA bases by non-enzymatic route.

Materials based on zero dimensions have attracted more attention in recent years due to their wide range applications [17, 18]. Nowadays, metal nanoparticles (MNPs) are widely used in various fields, especially for electrochemical sensors due to their excellent electrical conductivity, electroactive surface area, and so on [17–19]. Compared to other NPs and transition metal-based NPs, the AgNPs are inspired because of their high catalytic activity, and superior electrical conductivity [18, 20, 21]. During catalytic reactions, the metal-based nanoparticles showed an excellent electrocatalytic performance when anchored on suitable supporting substrates. However, the major limitation of MNPs is that they are unstable (strong aggregation) in natural environment without the stabilizing/capping agents, which eventually affects the catalytic activity [22, 23].

To minimize the stability and enhance catalytic activity, MNPs have been combined with active functional support materials. There are a variety of support materials that have been used for the different capping/stabilizing behavior of MNPs, including activated carbon, graphene-based materials, carbon nanomaterials, organic polymeric materials, metal–organic frameworks (MOFs), and so on [24–26]. Most of the above materials are expensive and require multi-step synthesis processes [24]. Moreover, inorganic-based functional materials provide limited catalytic activity because of their porous channels are poorly accessible for electrocatalytic activity [26, 27]. Although MOF-based materials have a huge specific surface area, they are not very stable in acidic environment due to the dissolution of ions. Therefore, it remains a great challenge to prepare a uniform dispersion of MNPs to keep them stable in an environment [26].

A new class of functional materials are COFs, which have been assembled from two different functional groups of lighter elements to form a framework structure [27–29]. COFs exhibit excellent physicochemical properties and a variety of applications such as gas storage, drug carrier and delivery, dye adsorption, energy storage, catalysis, and electrochemical/optical sensors [30]. However, the electrical conductivity of COF-based materials is limited due to their extended molecular structures [27, 28]. The advantage of the structural properties of COFs is that they act as host materials for MNPs and also play a strong adsorption anchor of MNPs and prevent the aggregation/agglomeration of individual MNPs. The chemical interaction between the MNPs and active heteroatom-containing COF not only fulfills the stability, but also improves the catalytic activity.

Here, we present a facile synthetic route for the development of AgNPs-embedded COF and then used for DNA base detection. The synthesized nanocomposite material was examined using various analytical techniques. The AgNPs-COF/GCE showed an excellent electrical conductivity, and faster electron transfer rate than unmodified, COF, and AgNPs-modified electrodes. The AuNPs-COF/GCE showed excellent catalytic performance for simultaneous, and individual detection of DNA bases, wide concentration range, low detection limit and acceptable interference-free performance.

Materials and methods

Chemicals and reagents

All chemicals and reagents are of analytical grade (99.00%). *p*-Phenylenediamine (*p*-PDA) (98.00%), terephthalaldehyde (99.00%), silver nitrate ($AgNO_3$) (≥ 99.00%), sodium borohydride ($NaBH_4$) (98.00%), purine guanine (G), adenine (A) and pyrimidine bases thymine (T), and cytosine (C) (98.00%) were obtained from Sigma Aldrich (https://www.sigmaaldrich.com). Anhydrous *N, N*-Dimethylformamide (DMF) (≥ 99.90%), sodium and disodium hydrogen phosphates ($NaHPO_4$) (≥ 99.00%) and (Na_2HPO_4) (≥ 99.00%) were obtained from Sigma Aldrich (https://www.sigmaaldrich.com). All interference compounds were obtained from Sigma Aldrich.

Instrumentations

FT–IR analysis was performed by JASCO FT–IR 6600 plus model, Japan. XRD analysis was performed using Ni-filtered Cu Kα (λ = 1.5406) radiation. The morphology of the synthesized nanocomposites was investigated using FE-SEM (F E I Quanta FEG 200 (15 kV)) and TEM (H-7600, Hitachi-Japan) at 200 kV. XPS analysis was performed by PHI 5000 Versa Probe II, FEI Inc. All electrochemical characterizations and electrocatalytic applications of purine and pyrimidine bases were performed using CHI electrochemical workstations (CHI6111E), USA with three electrode systems (glassy carbon-working, Ag/AgCl (sat NaCl)-reference,

Pt wire-counter electrode). The experimental parameters used for differential pulse voltammetry (DPV): Initial E (V) = 0.2; Final (V) = 0.6; Amplitude (V) = 0.05; Pulse width (sec) = 0.06; Sampling width (sec) = 0.02; Pulse period (sec) = 0.2 and Quiet time (sec) = 2. High-performance liquid chromatography (HPLC) was performed by using HP-1050 autosampler and detailed column/mobile phase and detectors are included in electronically supplementary material (ESI).

Synthesis of AgNPs—covalent organic framework (COF) composite

COF was synthesized as follows [30]. Briefly, 20 mM each of *p*-Phenylenediamine (0.0648 g) and terephthalaldehyde (0.0804 g) were completely dissolved in 30 mL of DMF using ultrasound (frequency–40 kHz). The reaction mixture (30 mL) was then transferred to a 50 mL round bottom flask with a reflux condenser for 12 h at 150 ± 1.3 °C under N_2 atmosphere. At the end of the reaction time, the temperature of reaction mixture was gradually cooled to ambient conditions (cooling rate = 2 °C/min). Then, the synthesized scaffold material was washed with an excess amount of DMF, and EtOH (three times) followed by drying hot oven at 80 °C for 4 h (Scheme 1).

Synthesis of AgNPs-embedded COF

The AgNPs-COF nanocomposite was prepared as follows. The synthesized *p*-Phenylenediamine-based COF material (0.2 mg/mL) was completely dispersed in 20 mL of deionized water (DI), and the mixture was constantly stirred for 2 h (750 RPM). Then, an aqueous solution of silver nitrate ($AgNO_3$) (25 mM) was added dropwise to the dispersed mixture and stirred for another 30 min. Finally, 100 µL of freshly prepared $NaBH_4$ (20 mM) was added dropwise until the color of the solution changed from colorless to light yellow due to the formation of Ag^0. Then, the nanocomposite material (AgNPs-COF) was washed repeatedly (about 5 times) with an excess amount of DI water and filtered, followed by drying (100 °C for 3 h).

Results and discussion

Choice of materials

Covalent organic frameworks (COFs) are a family of advanced functional materials composed of lighter elements (C, N, O, and B) [27]. COFs exhibit significant potential properties such as prefabricated structures, synthetically controllable pore sizes/volumes and functionally manageable, low density, extended surface area but limited electrical conductivity [28, 29]. Moreover, the combination of COF with MNPs, especially AgNPs, showed a remarkable improvement in physicochemical properties over the single compound due to a synergistic effect. DNA bases are an essential biomolecule, and responsible for gene information storage and bioprotein synthesis [2, 3]. The analytical significance of the quantitative determination of DNA bases was determined using AgNPs-COF.

Analysis of AgNPs-COF by spectral techniques

The functional group of the synthesized nanocomposite was evaluated by FT-IR. Figure S1 shows the FT-IR of *p*-Phenylenediamine (*p*-PDA), terephthalaldehyde, COF, and AgNPs-COF. The corresponding peaks and assignments are shown in ESI Table S1. Figure S1a shows the FT-IR of *p*-PDA, and peaks at 453, 1336, 1630, 3032, and

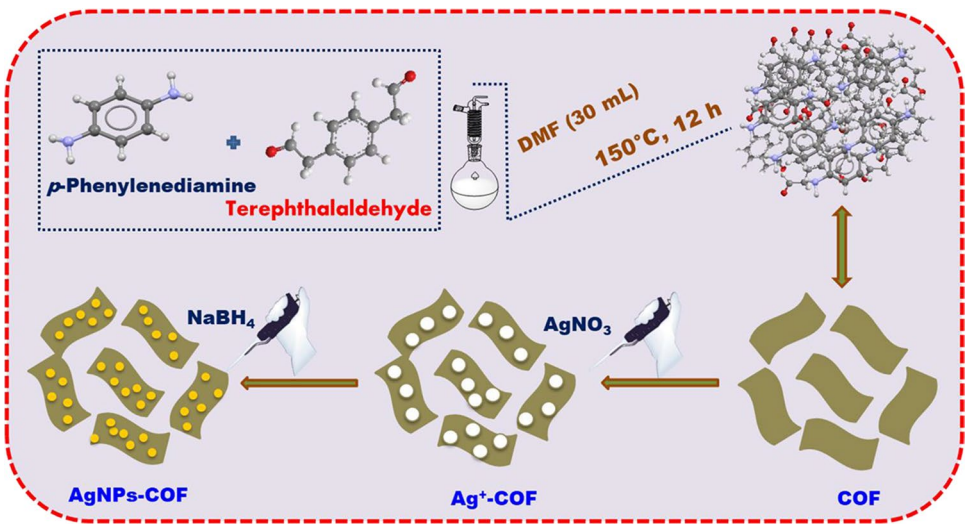

Scheme 1 Scheme showing the synthesis of AgNPs-COF

3271 cm^{-1} were detected. The peak at 453 cm^{-1} corresponds to the aromatic amine and 1336 and 1630 cm^{-1} are due to the symmetric vibrations of –C-N and –N–H, respectively [31]. The broad peak at 3032 and 3271 cm^{-1} is due to the symmetric and asymmetric vibration of –NH, respectively. Figure S1b shows the FT-IR spectrum of terephthalaldehyde and it showed peaks at 777, 815, 1195, 1302, and 1697 cm^{-1}, which are assigned to –C = C, –CH, –C–O, –C-H bending and –C = O, respectively [32, 33]. Figure S1c shows the FT-IR of COF. It shows the prominent new peaks compared to *p*-Phenylenediamine and terephthalaldehyde. The peaks were detected at 461, 742, 784, 1343, 1358, 1508, 1563, 1643, 3038, and 3281 cm^{-1}. The sharp peak at 742 is cm^{-1} responsible for –C-H and the newly discovered peak at 1563 cm^{-1} confirms the –C = N [30, 31, 33]. The peak at 3281 cm^{-1} is attributed to the stretching vibration of –NH for organic frameworks [31]. The AgNPs were embedded in COF and also showed similar stretching and bending vibrations with a slight shift in peak position for COF.

The crystalline behavior of AgNPs-COF was analyzed by XRD. Figure S2 shows the XRD pattern of COF, which shows a peak at 20.92° (0 0 2) which can be attributed to the crystalline plane of COF. Moreover, the AgNPs-COF showed distinguishable peaks at 38.02°, 44.22°, 64.97°, and 77.47° are corresponding to the respective (1 1 1), (2 0 0), (2 2 0), and (3 1 1) crystal planes of AgNPs [34]. The XPS is a powerful analytical tool for the detailed information about the electronic states and chemical bonding environments of AgNPs-COF. Figure S3A shows the XPS survey spectrum, which yields three binding energies, including C1s, N1s, and Ag3d. Figure S3B shows the C1s spectrum, which reveals three subpeaks at 284.5, 286.3, and 287.8 eV equivalent to –C = C, –C-N and –C = N, respectively [35]. The deconvoluted N1s peaks at 397.2, 398.5, and 399.1 eV are assigned to = N–, –C = N, and –NH, respectively [35] (Fig. S3C). Figure S3D displays the XPS spectrum of Ag3d. It shows the binding energies at 367.8, and 373.8 eV for $Ag3d_{3/2,}$ and $Ag3d_{5/2}$, respectively [34].

Evaluation of AgNPs-COF by microscopic techniques

Figure 1 shows the TEM image of COF and provides the sheet-like morphological structure. Each morphological structure has very thin layers. Figures 1b, c, d show the

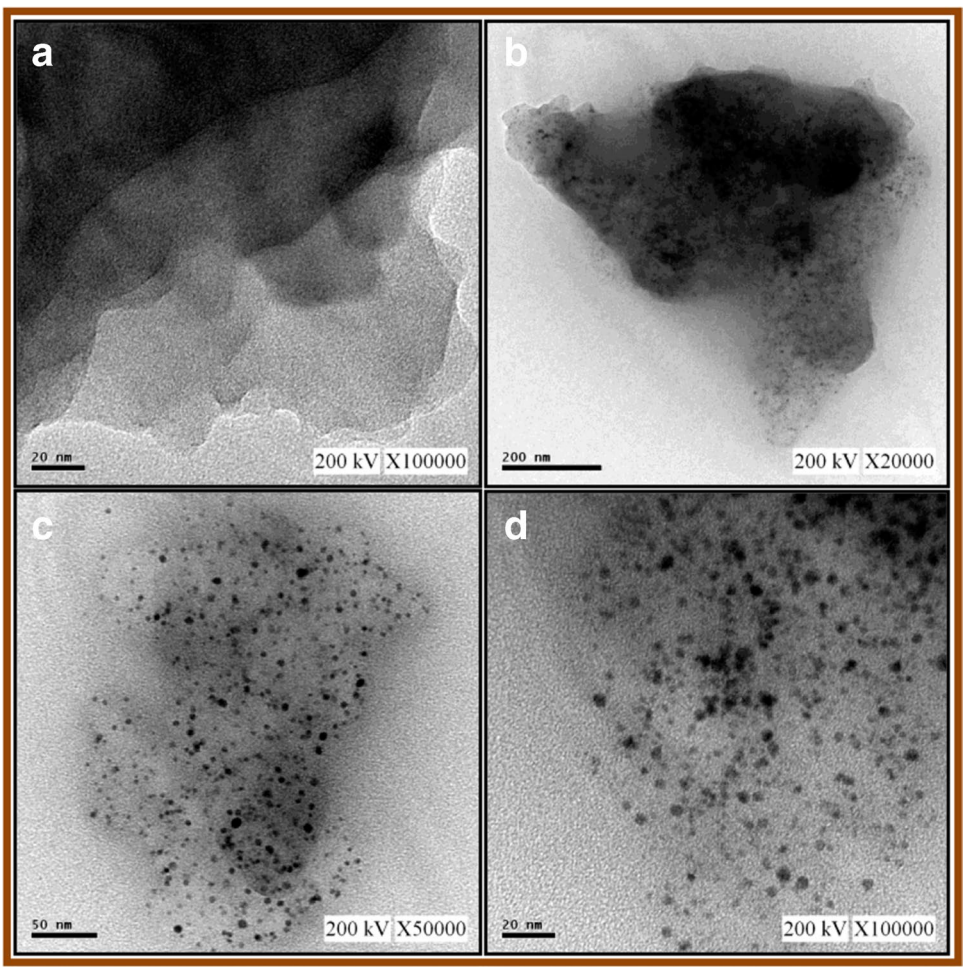

Fig. 1 TEM images of COF (**a**), AgNPs-COF (**b**, **c** and **d**) with higher magnifications

COF embedded in AgNPs with three higher magnifications. Interestingly, very small spherical AgNPs were embedded in COF and each particle has the same morphological dimensions. The average particle size of the synthesized AgNPs was 2.1 ± 0.04 nm (n = 28). Moreover, the obtained morphological structure, and particle size distribution were again confirmed by FE-SEM. Figure S4 shows the FE-SEM images of COF, and AgNPs-COF. They show the sheet-like structures of COF and the spherical AgNPs in COF. The obtained FE-SEM morphological structure with particle sizes agreed well with the TEM studies.

Subsequently, the elemental composition of the synthesized AgNPs-COF was characterized by EDX. Figure S5 shows the EDX spectrum of AgNPs-COF and reveals different binding energies at 0.227, 0.392, and 0.525 keV due to the confirmation of Kα-energy shells of carbon, nitrogen, and oxygen, respectively. The oxygen peak obtained could be due to the water molecules adsorbed on the synthesized material from the atmospheric environment. In addition, two distinct peaks at 22.163 and 2.963 keV were detected, confirming that Ag has two distinct energy shells, including Kα and Lα.

Electrochemical behavior of AgNPs-COF on GC electrode

The redox behavior of AgNPs-COF/GCE was characterized by cyclic voltammetry (CV) in 0.2 M PBS (Fig. S6). No redox response was detected at COF/GCE due to the absence of electroactive functional group. Besides, the AgNPs-COF/GCE showed a broad peak. The oxidation peak was delivered at E_{pa} of + 0.15 V and the subsequent reduction peak at E_{pc} of + 0.04 V, which can be attributed to the characteristic behavior of Ag^0 to Ag^+ and Ag^+ to Ag^0 [34]. The result of CV clearly shows that the AgNPs were successfully embedded in COF.

The electrical conductivity of the modified electrode was further evaluated by EIS in 5 mM $K_3/K_4[Fe(CN)_6]$ in 0.1 M KCl at various frequencies from 0.01 to 100,000 Hz. Figure S7 shows the Nyquist plots for control and modified electrodes on bare GCE, COF, and AgNPs-COF/GCEs. The obtained data were well fitted with a Randles circuit model (*inset*). The plots were fitted with real (Z') and unreal axis (Z'') and all peaks showed a well-defined semicircular region with a tail group. The obtained R_{ct} values of 518, 432, and 321 Ω are components with the bare GCE, COF, and AgNPs-COF/GCEs, respectively. Next, k_{et} was calculated based on Eq. (1) [34, 35].

$$k_{et} = RT/n^2F^2AR_{CT}C^o \quad (1)$$

where, R, T, F, A, C^o have their usual meaning. The calculated k_{et} values of the different modified electrodes are 0.78, 0.92 and 1.38×10^{-4} cm^2 s^{-1}. The modified nanocomposite electrode has 1.7 and 1.5 times higher electrical conductivity than the control electrodes, and AgNPs/GCE. Then, the EASA of the fabricated electrodes was measured using Randles–Sevcik Eq. (2) [35].

$$I_p = 2.69 \times 10^5 n^{3/2} AD^{1/2} C\upsilon^{1/2} \quad (2)$$

where I_p, A, D, C, n and ν are the current, the electrode surface area (cm^2), the diffusion co-efficient of ($K_3[Fe(CN)_6]$), the redox probe concentration, number of electron transfers and scan rate, respectively. According to Eq. (2), the measured EASA for the different electrodes is 0.063, 0.135, 0.202, and 0.372 cm^2 for the bare GCE, COF, AgNPs, and AgNPs-COF/GCEs, respectively. The nanocomposite modified electrode (AgNPs-COF) showed an easier electron transfer rate constant than the bare GCE, AgNPs, and COF modified electrodes.

Electrocatalytic behavior of DNA bases

Electrochemical behavior of G, A, T and C on modified electrodes

Figure 2 shows the DPV for 10 µM each of G, A, T, and C at the unmodified electrode surface, and reveals broad oxidation peaks with less intense peak currents at E_{pa} of + 0.65, + 0.94, and + 1.31 V, respectively for G, A, and the combination of T and C (single peak). The lower oxidation current response is responsible for arises from limited kinetics of the rate transition, and it is impossible to use the bare GCE to measure G, A, T and C, simultaneously (Fig. 2A).

Moreover, the COF/GCE showed less pronounced oxidation peak currents with peak potentials at E_{pa} of + 0.61, + 0.89, + 1.13, and + 1.28 V for G, A, T, and C, respectively (Fig. 2B). On the other hand, the AgNPs/GCE show oxidation peak potentials at + 0.63, + 0.90, + 1.12 and + 1.28 V for G, A, T and C, respectively, with acceptable oxidation current profiles (Fig. S8). Next, a well-distinguishable peak and currents (oxidation) were detected at the electrode modified with the nanocomposite (AgNPs-COF/GCE). A separate peak was delivered at E_{pa} of + 0.63, + 0.89, + 1.10 and + 1.26 V with oxidation peak current I_{pa} of 7.12, 5.02, 1.13, and 1.26 µA for G, A, T, and C, respectively (Fig. 2C). Compared with the modified/unmodified electrodes, the AgNPs-COF/GCE showed better DNA base catalytic activity, including peak oxidation currents, peak shape, and potentials, due to the facile electron transfer rate constant/electrical conductivity, and the synergistic effect of the MNPs with base material than others (Fig. 2D). The detailed effects of $AgNO_3$ concentration in AgNPs-COF and loading level of electrocatalyst

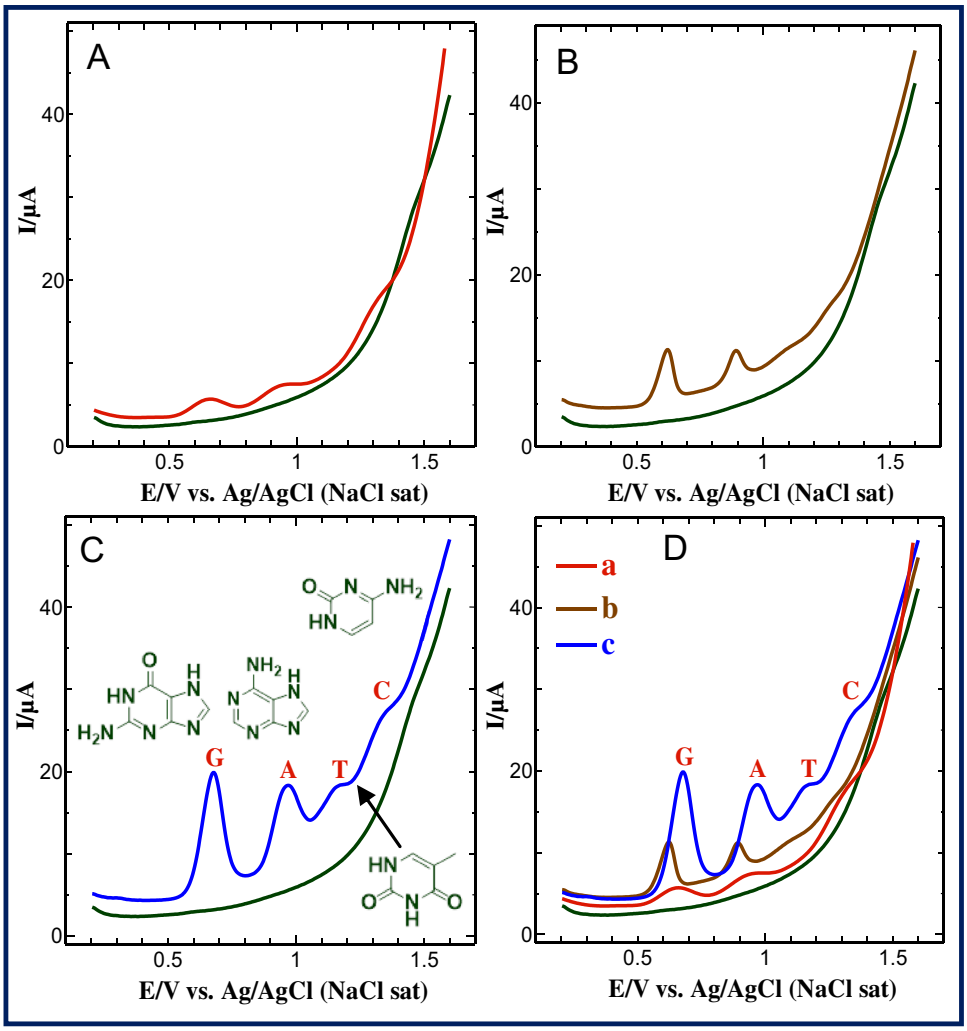

Fig. 2 DPVs for the determination of each 10 μM G, A, T, and C on unmodified GCE (**A**) COF (**B**) and AgNPs-COF modified GC electrodes (**C**) in 0.2 M PB solution (pH 7.0) and comparative DPVs curves of modified and control electrodes (**D**) (a- unmodified; b- COF, c- AgNPs-COF/GCEs)

(AgNPs-COF) are given in the electronically supplementary material (ESI) (Figs. S9 and S10).

Effect of supporting electrolyte (pH)

Figure S11A shows the effect of supporting electrolytes in terms of currents, and the potentials of G, A, T and C on AgNPs-COF/GCE in PBS. When the pH was increased from 4.0 to 9.0, the peak potential shifted toward the less positive region due to the proton transfer process [2]. Moreover, the peak current of purine and pyrimidine bases increased from pH 4.0 to 7.0, while the current at pH 8.0 and 9.0 was decreased due to the limitation of protons in the electrochemical oxidation reaction. Based on the pH effect, the maximum oxidation current was found to be at pH 7.0, mimicking the characteristic behavior of neutral pH. Hence, pH 7.0 was optimized for all electrochemical sensing applications of DNA bases. Figure S11B shows the plot of current against the potentials (peak) of G, A, T, and C. The linear plots and calculated values were 0.057, 0.060, 0.056, and 0.062 V/pH, respectively (Eqs. (3), (4), (5), (6), which is closely related to Nernst theoretical value (0.059 V/pH) at 25 °C and confirms that the oxidation behavior of DNA bases proceeds with the same number of electrons and protons [14].

$$E_{pa}(G) = -0.057pH + 1.024(R^2 = 0.996) \quad (3)$$

$$E_{pa}(A) = -0.060pH + 1.184(R^2 = 0.990) \quad (4)$$

$$E_{pa}(T) = -0.056pH + 1.348(R^2 = 0.986) \quad (5)$$

$$E_{pa}(C) = -0.062pH + 1.452(R^2 = 0.989) \quad (6)$$

The plausible mechanism of the oxidation reaction of purine and pyrimidine bases based on the different pH values of the electrolyte solution could be due to the diversity of their chemical structures. Scheme S1 shows the

oxidation mechanism of DNA bases on a modified electrocatalyst (AgNPs-COF/GCE), and it shows that the system has a complex process [36].

Sensitive determination of G, A, T, and C by DPV

Before proceeding to the simultaneous determination of DNA bases, the specific oxidation behavior of G, A, T, and C was first investigated using DPV based on AgNPs-COF/GCE. Figure 3 shows the DPVs for 3 µM each of G, A, T, and C on AgNPs-COF/GCE under an optimized working parameter. No current responses were observed in the absence of each analyte. On the other hand, the peaks were delivered at E_{pa} of + 0.63, + 0.89, + 1.10, and + 1.26 V for G, A, T, and C, respectively, while the presence of 3 µM each (curve a). When the concentrations 6 to 24 µM of each G, A, T, and C were increased, the oxidation peak current responses were increased (curves b to h). The well-formed and stable currents of G, A, T, and C clearly indicated that AgNPs-COF/GCE could be successfully used for the specific and stable determination of DNA bases.

Selective electrochemical oxidation of G, A, T and C by DPV

The DPV technique is used for specific and simultaneous detection of DNA bases because it has high sensitivity, a sharp oxidation peak, and faster responses than CV. Figure 4A expresses the DPV for each 3 µM G in the fourfold excess concentrations of A, T, and C in 0.2 M PBS and it was found that the oxidation peaks were detected at E_{pa} of + 0.63 V (G), + 0.89 V (A), + 1.10 V (T), and + 1.27 V (C). While the analyte of G was increased from 6 to 24 µM, the current response increased at a similar peak potential (curves a–h). On the other hand, the peak current of A, T, and C was not significantly changed. The current versus analyte response of G is straight-line and is given as Eq. (7) (Fig. 4B). Figure 4C shows the DPV for 3 µM of A in 12 µM of G, T, and C. It shows the current at E_{pa} of + 0.89 V and the response was significantly increased by the addition of A (curves a–h). The result of the plot of A is straight-line and the regression co-efficient is given as Eq. 8 (Fig. 4D).

$$I_{pa}\mathrm{G}(\mu\mathrm{A}) = 4.9458[\mathrm{G}](\mu\mathrm{M}) + 0.4496\left(\mathrm{R}^2 = 0.9974\right) \quad (7)$$

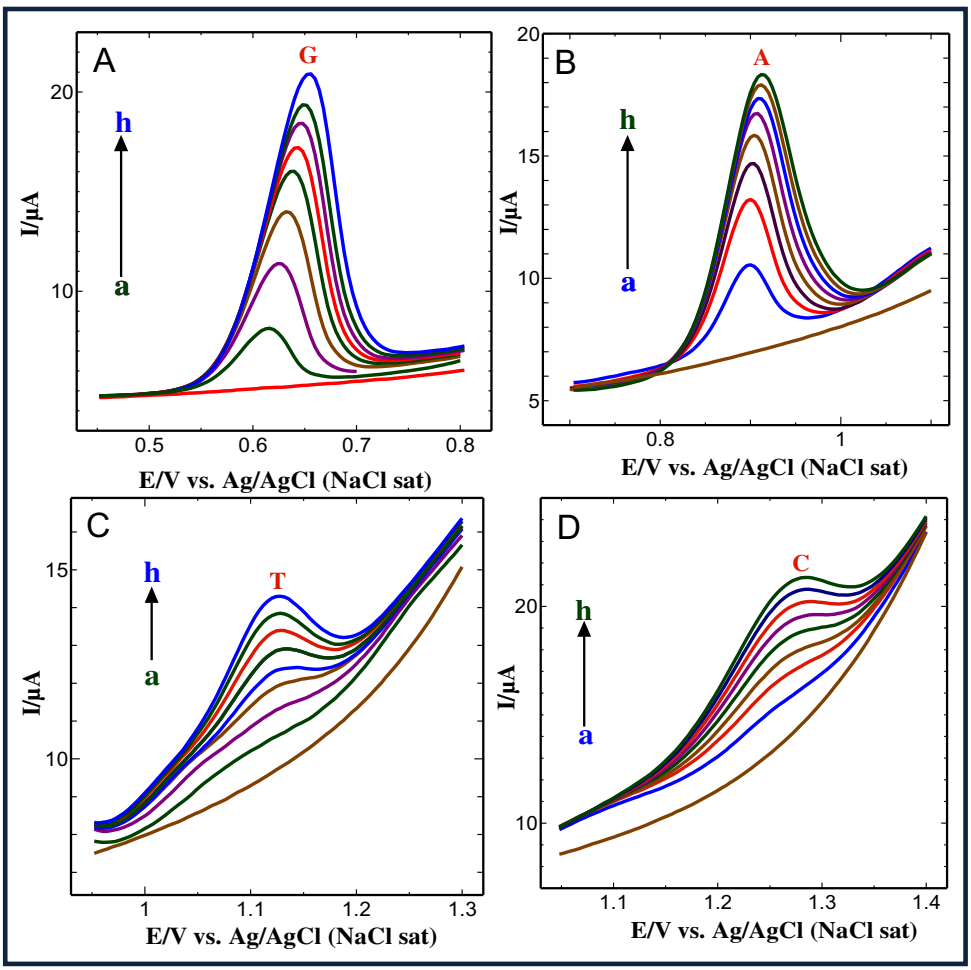

Fig. 3 DPVs obtained for G, A, T, and C on AgNPs-COF/GCE in 0.2 M PB solution (pH 7.0). Each addition of G, A, T and C increased the concentration by 3 µM (a–h)

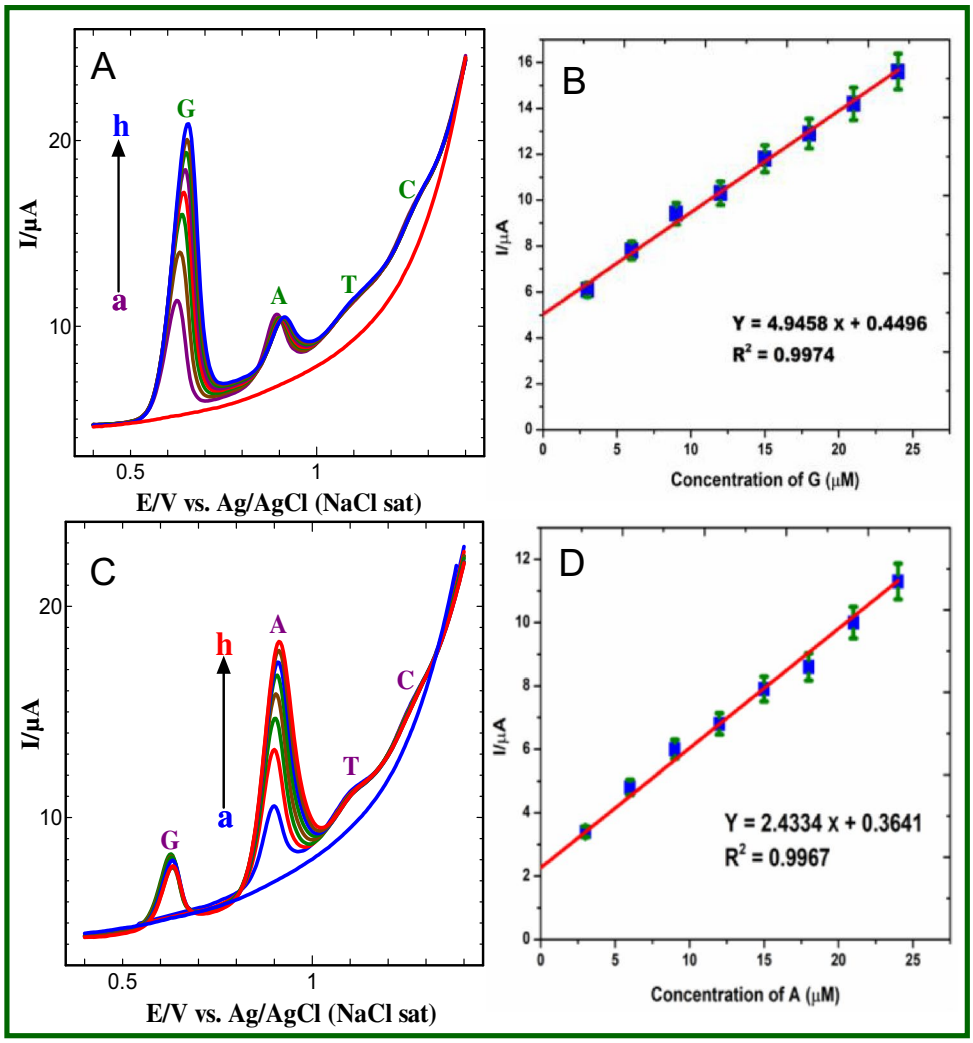

Fig. 4 (**A**) DPVs for each 3 μM of G to 12 μM of A, T and C (curves a–h) on AgNPs-COF/GC electrode. (**C**) DPVs for each 3 μM of A to 12 μM of G, T and C (curves a–h) on AgNPs- COF/GCE. (**B**) and (**D**) Plot of concentration of G and A vs. oxidation current

$$I_{pa}\mathrm{A}(\mu\mathrm{A}) = 2.4334[\mathrm{A}](\mu\mathrm{M}) + 0.3641(\mathrm{R}^2 = 0.9967) \quad (8)$$

Figure 5A shows the DPV for 3 μM T in a mixture of G, A and C in 0.2 M PBS. The peak was observed at E_{pa} of + 1.10 V due to oxidation of T and peaks were observed at E_{pa} of + 0.63, + 0.89, and + 1.26 V for 3 μM of G, A, and C, respectively. While the analyte of T (6–24 μM) increased (curves a–h), the obtained current increased in a mixture with other DNA bases. The plot of the current against the analyte of T is straight-line and corresponds to Eq. (9) (Fig. 5B). Figure 5C shows the selective determination of C in the presence of the other DNA bases (G, A, and T). The oxidation peak current was detected at E_{pa} of + 1.26 V due to the oxidation behavior of 3 μM C in a mixture containing the analytes (G, A, and T). Upon increasing the analyte of C, the current responses were linearly increased (curves a–h). The current versus analyte C is straight-line and is given as Eq. (10) (Fig. 5D).

$$I_{pa}\mathrm{T}(\mu\mathrm{A}) = 0.1259[\mathrm{T}](\mu\mathrm{M}) + 0.2337(\mathrm{R}^2 = 0.9979) \quad (9)$$

$$I_{pa}\mathrm{C}(\mu\mathrm{A}) = 0.6382[\mathrm{C}](\mu\mathrm{M}) + 0.2446(\mathrm{R}^2 = 0.9961) \quad (10)$$

Simultaneous oxidation behavior of G, A, T and C by DPV

Another important goal of the present study is the simultaneous analysis of G, A, T and C in the physiological environment at the modified electrocatalyst. Figure 6A shows the DPVs for 3 μM each of G, A, T, and C. Peak currents were observed at E_{pa} of + 0.63, + 0.89, + 1.10, and + 1.26 V, respectively. While the concentrations of purine (G and A), and pyrimidine (T and C) bases were increased, the oxidation peak currents increased significantly as a function of concentrations. On the other hand, the peak potential did not change with the addition of each analyte. Figure 6B shows the bar plot for the current of G, A, T and C as a function of concentrations. Based on the sensitivity of the analytes, the increasing order of the peak current is G > A > C > T.

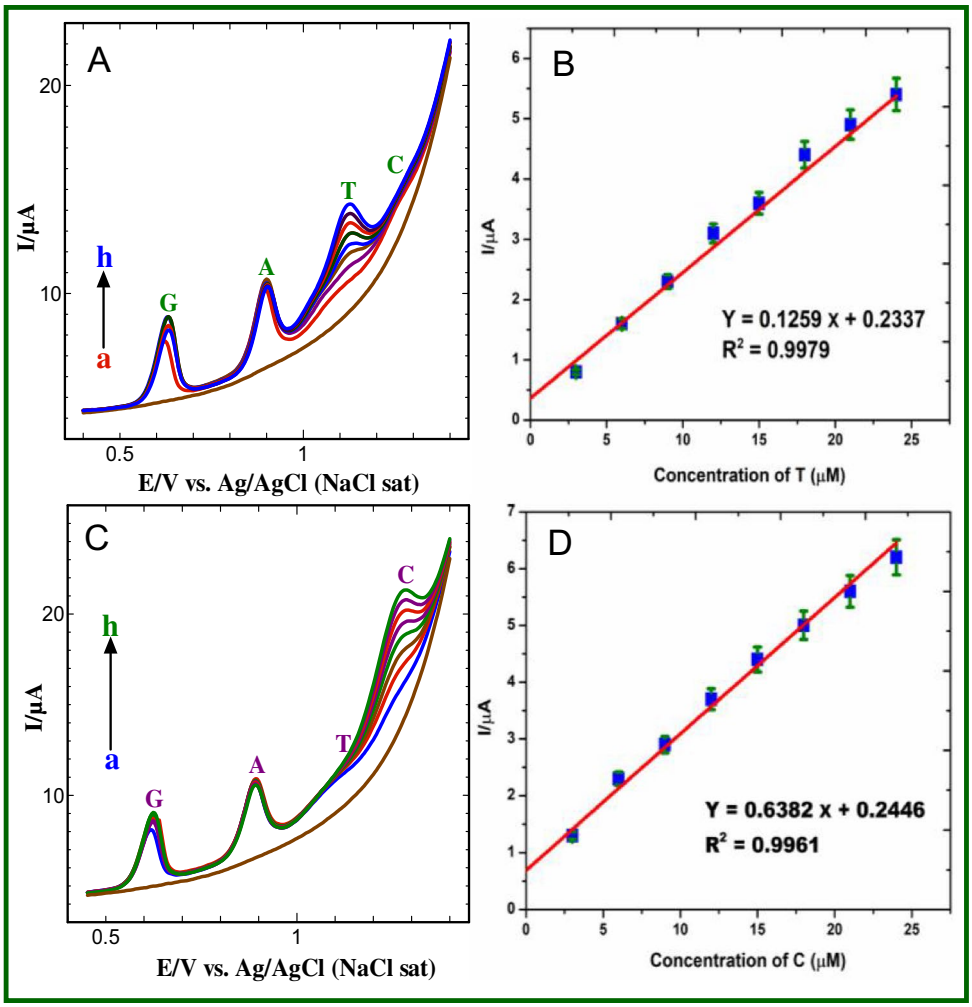

Fig. 5 (**A**) DPVs for each 3 μM of T to 12 μM of G, A and C (curves a–h) on AgNPs-COF/GC electrode. (**C**) DPVs for each 3 μM of C to 12 μM of G, A and T (curves a–h) on AgNPs- COF/GCE. (**B**) and (**D**). Plot of concentration of T and C vs. oxidation current

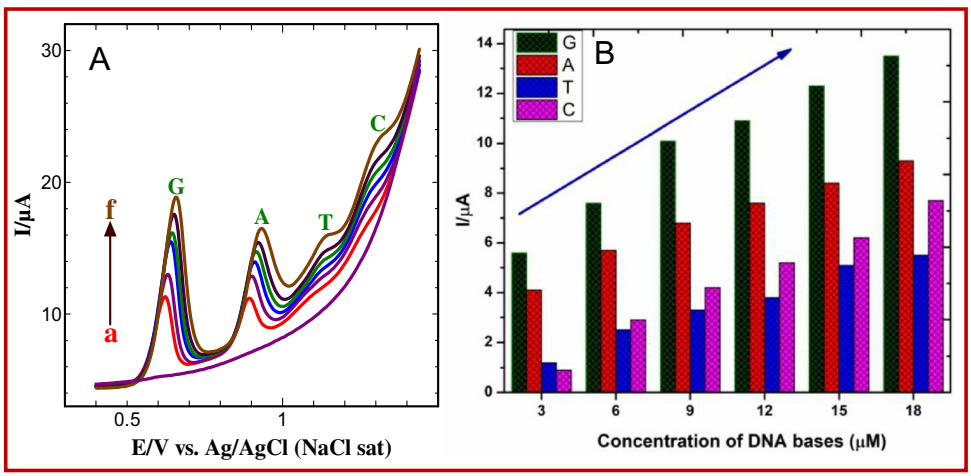

Fig. 6 (**A**) DPVs for each addition of 3 μM G, A, T, and C (curves a–f) at AgNPs-COF/GCE in 0.2 M PB solution (pH 7.0). (**B**). Bar graph profile for current vs. concentration of DNA bases

Sensitive determination of G, A, T, and C by amperometry

The amp *i-t* curve for sensitive measurement of DNA bases is an effective and rapid detection technique because it is highly sensitive, responds quickly, and minimizes electrode passivation. Figure 7A shows the amp *i-t* curve for the sensitive measurements of G with an optimized applied potential and a time interval of 50 s under constant stirring conditions. As the concentration of G increased, the oxidation peak current was increased significantly from nanomolar to millimolar

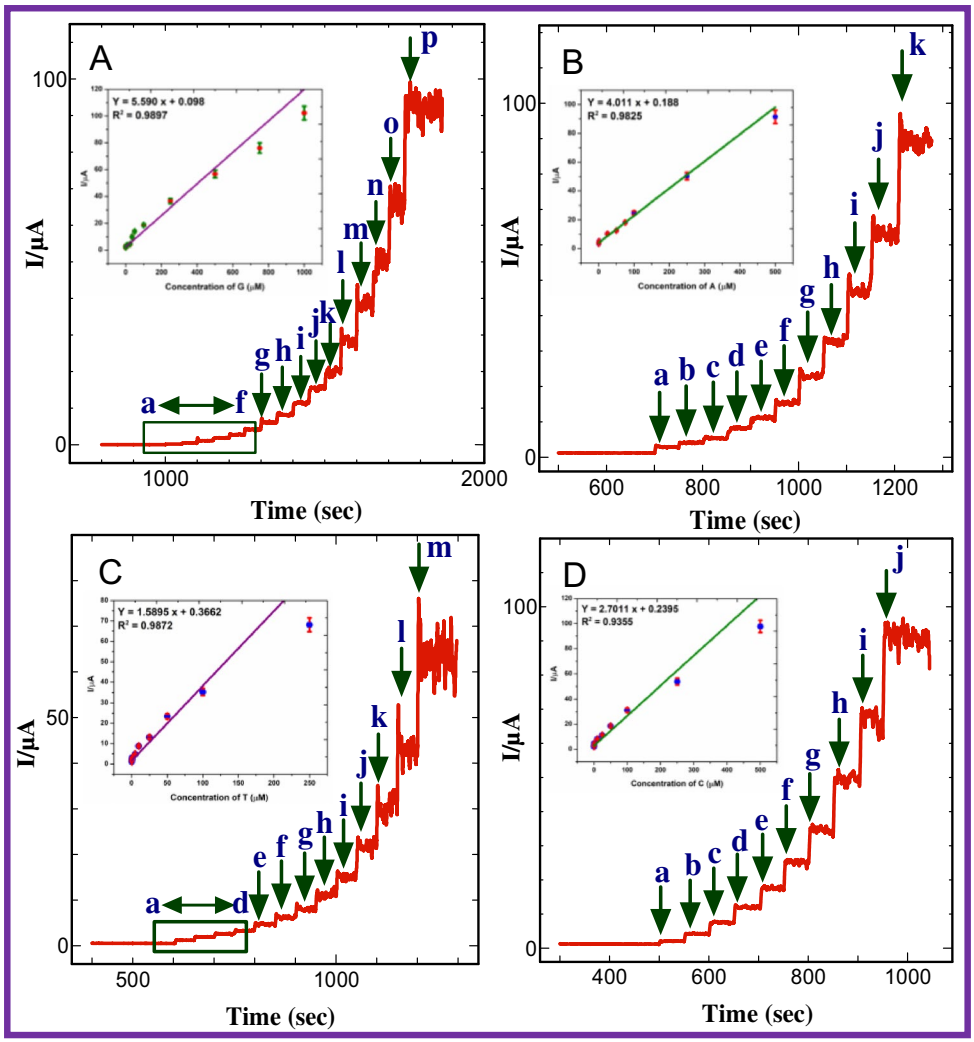

Fig. 7 Amperometric *i-t* curve for the determination of G, A, T, and C on AgNPs-COF/GCE in 0.2 M PBS (pH 7.0). (**A**) **G** – 0.20 (a), 0.50 (b), 0.10 (c), 0.25 (d), 0.50 (e), 1 (f), 5 (g), 10 (h), 25 (i), 35 (j), 50 (k), 100 (l), 250 (m), 500 (n), 750 (o), and 1000 (p) μM. (**B**) **A** – 0.10 (a), 0.25 (b), 0.50 (c), 0.75 (d), 1 (e), 25 (f), 50 (g), 75 (h), 100 (i), 250 (j), 500 (k) μM. (**C**) **T** – 0.25 (a), 0.35 (b), 0.50 (c), 0.60 (d), 0.75 (e), 0.85 (f), 1 (g), 5 (h), 10 (i), 25 (j), 50 (k), 100 (l), 250 (m) μM. (**D**) **C** – 0.15 (a), 0.30 (b), 0.50 (c), 1 (d), 10 (e), 25 (f), 50 (g), 100 (h), 250 (i), 500 (j) μM. *Insets*: Calibration plot of current vs. concentration of G, A, T, and C

(200 nM to 1 mM), and no significant peak noise was detected. The curve of current versus analyte G is straight-line and the coefficient is given in Eq. (11). In addition, analytes A, T, and C were increased from 100 nM to 500 μM, 250 nM to 250 μM, and 150 nM to 500 μM, respectively, when the current was increased (Fig. 7B, C and D). The plot of current vs. analytes of A, T and C is straight-line and the correlation coefficient is given in Eqs. (12), (13), and (14).

$$I_{pa}G(\mu A) = 5.5902G\ (\mu M) + 0.0983(R^2 = 0.9897) \quad (11)$$

$$I_{pa}A(\mu A) = 4.0112A\ (\mu M) + 0.1880(R^2 = 0.9825) \quad (12)$$

$$I_{pa}T(\mu A) = 1.5895T\ (\mu M) + 0.3662(R^2 = 0.9872) \quad (13)$$

$$I_{pa}C(\mu A) = 2.7011C\ (\mu M) + 0.2395(R^2 = 0.9355) \quad (14)$$

Furthermore, the LOD was calculated from the standard method as following Eq. (15)

$$LOD = 3\sigma/slope \quad (15)$$

where the σ-value was derived from the background currents of the amp *i-t* curve (12 times repeated measurements) and the slope value was derived from the amp *i-t* curve. The calculated LODs were 0.043, 0.056, 0.062, and 0.051 μM (S/N = 3) for G, A, T and C, respectively. The obtained linear results of the present sensor for a wide range and LOD were compared with the published research papers are summarized in Table S2 [11, 13, 15, 36–38] and it was found that the present sensor exhibited superior electrocatalytic activity.

Anti-interference study of G, A, T and C

Anti-interference study was performed by selectively measuring the G, A, T and C in other possible interferences such

as uric acid, ascorbic acid, dopamine, serotonin, norepinephrine, Ca^{2+}, Cu^{2+}, Zn^{2+}, Mg^{2+}, and Fe^{3+} on the AgNPs-COF/GCE by DPVs (Fig. S12). During the addition of 10 µL of each DNA bases to the working electrolyte, the current response was improved (curve a). Then, when a 15-fold higher amount of the biologically relevant molecules uric acid (curve b), ascorbic acid (curve c), and dopamine (curve d) were added to the mixture with DNA bases, the current behavior did not significantly change. In addition, 25-fold higher concentrations of serotonin (curve e), norepinephrine (curve f), Ca^{2+} (curve g), Cu^{2+} (curve h), Zn^{2+} (curve i), Mg^{2+} (curve j), and Fe^{3+} (curve k) were added to the same mixture, and the current responses of G, A, T, and C were not significantly improved. The interference results obtained clearly confirmed that the present electrocatalyst was successfully used for the selective measurement of G, A, T and C in a potentially important biological compound containing amine and metal ion species.

Effect of stability, and reproducibility

The stability and reproducibility of the present sensor was investigated by DPV at AgNPs-COF/GCE (Fig. S13). To confirm the reproducibility of the present sensor, 10 µM of G, A, T and C were measured in 0.2 M PBS (pH 7.0) at five independent modified electrodes (curves a–e). The oxidation peak currents of G, A, T, and C were almost similar with low error percentages of 1.23 ± 0.02%, 1.83 ± 0.04%, 1.53 ± 0.08%, 1.34 ± 0.12%, and 1.64 ± 0.08%, respectively. The obtained DPV results clearly indicate that the present sensor has acceptable reproducibility. The obtained relative standard deviation (RSD) of five different modified electrodes as 2.58 ± 0.02%, 1.67 ± 0.03%, 3.04 ± 0.05%, 1.53 ± 0.04% and 2.14 ± 0.03% (n = 3), respectively. Moreover, the stability of the present sensor was measured from one to five days by DPV and the rest of the time the modified nanocomposite electrode was stored at room temperature. The oxidation peak potentials were found at E_{pa} of + 0.63, + 0.89, + 1.10 and + 1.26 V for 10 µM of G, A, T and C respectively. When the storage time was increased from two to five days, the oxidation currents and peak potentials were obtained similar and the RSD values ranged from 1.22 ± 0.06% to 2.15 ± 0.04% (n = 3).

Analysis of practical application

Practical application was demonstrated in blood serum (human), urine and saliva samples at AgNPs-COF/GCE in physiological environment. All blood serum and urine samples were collected from the Reputed medical testing laboratory, Taiwan. The human saliva samples were collected by laboratory co-workers. The collected samples were diluted tenfold to control the matrix effect of the real biological sample, and without any further free-treatments. In the absence and presence of blood serum, urine, and saliva samples, no actual response was detected. In addition, a known amount of 10 µM of G, A, T and C was added to the mixture with the real samples, and the peaks were delivered at E_{pa} of + 0.63, + 0.90, + 1.10 and + 1.27 V, respectively. Furthermore, the standard addition method was used for the quantitative measurements of DNA bases. The detailed results and recovery concentrations of G, A, T and C and are shown in Table S3 and the acceptable recovery percentages are 98.603–99.112%, 97.802–99.211%, 98.693–99.742% for practical samples, respectively. The obtained voltammetry results propose that the present sensor has been successfully used for the quantitative measures of DNA bases. Finally, the electrochemical results were validated with the standard analytical method of HPLC and the results obtained are good and satisfactory with acceptable error percentages (Table S4).

Conclusions

AgNPs-COF modified GCE used for sensitive, and simultaneous measurements of DNA bases was developed in physiological environment (pH = 7.0; PBS). The nanocomposite material was synthesized by reflux followed by stirring in an optimized chemical quantity. The AgNPs-COF was characterized by different analytical techniques. Moreover, the electrocatalyst (AgNPs-COF) was modified on a clean GCE and then used for simultaneous and selective measurement of DNA bases. The present sensor delivered wide concentration range, low detection limit, interference free, high stability and reproducibility toward G, T, A and C. Finally, the present electrocatalyst was used for quantitative detection of DNA bases in biologically relevant samples and subsequently validated by HPLC method.

Supplementary Information The online version contains supplementary material available at https://doi.org/10.1007/s00604-021-05021-7.

Funding The authors are grateful for the financial support from the Ministry of Science and Technology, Taiwan (MOST-107–2113-M-027–006 and MOST-108–2113-M-027–001). P. Arul would like to express gratitude to the National Taipei University of Technology for the Post-doctoral fellowship.

Declarations

Conflict of interest The authors declare no competing interests.

References

1. Watson JD, Crick FHC (1953) Molecular structure of nucleic acids: a structure for deoxyribose nucleic acid. Nature 171:737–738

2. Lavanya N, Claude JN, Sekar C (2018) Electrochemical determination of purine and pyrimidine bases using copper doped cerium oxide nanoparticles. J Colloid Interface Sci 530:202–211
3. Yari A, Saidikhah M (2016) Trithiane silver-nanoparticles-decorated polyaniline nanofibers as sensing element for electrochemical determination of Adenine and Guanine in DNA. J Electroanal Chem 783:288–294
4. Li T, Li B, Dong S (2007) Aptamer-based label-free method for hemin recognition and DNA assay by capillary electrophoresis with chemiluminescence detection. Anal Bioanal Chem 389:887–893
5. Qian Y, Fan T, Yao Y, Shi X, Liao X, Zhou F, Gao F (2018) Label-free and Raman dyes-free surface-enhanced Raman spectroscopy for detection of DNA. Sens Actuators B Chem 254:483–489
6. Doshi R, Day PJR, Carampin P, Blanch E, Stratford IJ, Tirelli N (2010) Spectrophotometric analysis of nucleic acids: oxygenation-dependant hyperchromism of DNA. Anal Bioanal Chem 396:2331–2339
7. Fujimura YK, Komatsu Y, Kuraishi H, Kaneko T (1984) Estimation of DNA base composition by high performance liquid chromatography of its nuclease pi hydrolysate. Agric BioI Chem 48:3169–3172
8. Rehman A, Jenner A, Halliwell B (2000) Gas chromatography-mass spectrometry analysis of DNA: optimization of protocols for isolation and analysis of DNA from human blood. Methods Enzymol 319:401–417
9. Yeh CF, Jiang SJ (2002) Determination of monophosphate nucleotides by capillary electrophoresis inductively coupled plasma mass spectrometry. Analyst 127:1324–1327
10. Brooks SC, Richter MM (2002) Determination of DNA bases using electrochemistry: a discovery-based experiment. Chem Educat 7:284–287
11. Sadeghi M, Jahanshahi M, Javadian H (2020) Highly sensitive biosensor for detection of DNA nucleobases: enhanced electrochemical sensing based on polyaniline/single-layer MoS_2 nanosheets nanocomposite modified carbon paste electrode. Microchem J. 152:104315
12. Lei P, Zhou Y, Zhu R, Liu Y, Dong C, Shuang S (2020) Novel strategy of electrochemical analysis of DNA bases with enhanced performance based on copper nickel nanosphere decorated N, B doped reduced graphene oxide. Biosens Bioelectron 147:111735
13. Wang S, Ferrag C, Noroozifar M, Kerman K (2020) Simultaneous determination of four DNA bases at graphene oxide/multi-walled carbon nanotube nanocomposite-modified electrode. Micromachines 11:294
14. Wang X, Zhang J, Wei Y, Xing T, Cao T, Wu S, Zhu F (2020) A copper-based metal–organic framework/graphene nanocomposite for the sensitive and stable electrochemical detection of DNA bases. Analyst 145:1933–1942
15. Deng C, Xia Y, Xiao C, Nie Z, Yang M, Si S (2012) Electrochemical oxidation of purine and pyrimidine bases based on the boron-doped nanotubes modified electrode. Biosens and Bioelectron 31:469–474
16. Wang L, Yu F, Wang F, Chen Z (2016) Electrochemical detection of DNA methylation using a glassy carbon electrode modified with a composite made from carbon nanotubes and β-cyclodextrin. J Solid State Electrochem 20:1263–1270
17. Wu K, Fei J, Bai W, Hu S (2003) Direct electrochemistry of DNA, guanine and adenine at a nanostructured film-modified electrode. Anal Bioanal Chem 376:205–209
18. Luo X, Morrin A, Killard AJ, Smyth MR (2006) Application of nanoparticles in electrochemical sensors and biosensors. Electroanalysis 18:319–326
19. Wang J (2012) Electrochemical biosensing based on noble metal nanoparticles. Microchim Acta 177:245–270
20. Mavaei M, Chahardoli A, Shokoohinia Y, Khoshroo A, Fattahi A (2020) One-step synthesized silver nanoparticles using isoimperatorin: evaluation of photocatalytic, and electrochemical activities. Sci Rep 10:1762
21. Lu L, Hu X, Zhu Z, Li D, Tian S, Chen Z (2020) Review-Electrochemical sensors and biosensors modified with binary nanocomposite for food safety. J Electrochem Soc 167:037512
22. Manojkumar K, Sivaramakrishna A, Vijayakrishna K (2016) A short review on stable metal nanoparticles using ionic liquids, supported ionic liquids, and poly(ionic liquids). J Nanopart Res 18:103
23. Pan M, Yang J, Liu K, Yin Z, Ma T, Liu S, Xu L, Wang S (2020) Noble metal nanostructured materials for chemical and biosensing systems. Nanomater 10:209
24. Xie F, Yang M, Jiang M, Huang XJ, Liu WQ, Xie PH (2019) Carbon-based nanomaterials A promising electrochemical sensor toward persistent toxic substance. Trends Anal Chem 119:115624
25. Wu S, He Q, Tan C, Wang Y, Zhang H (2013) Graphene-based electrochemical sensors. Small 9:1160–1172
26. Liu CS, Li J, Pang H (2020) Metal-organic framework-based materials as an emerging platform for advanced electrochemical sensing. Coord Chem Rev 410:213222
27. Zhang J, Tan Y, Song WJ (2020) Zeolitic imidazolate frameworks for use in electrochemical and optical chemical sensing and biosensing: a review. Microchim Acta 187:234
28. Geng K, He T, Liu R, Dalapati S, Tan KT, Li Z, Tao S, Gong Y, Jiang Q, Jiang D (2020) Covalent organic frameworks: design, synthesis, and functions. Chem Rev 120:8814–8933
29. Lohse MS, Bein T (2018) Covalent organic frameworks: structures, synthesis, and applications. Adv Funct Mater 28:1705553
30. Gomes R, Bhanja P, Bhaumik A (2015) A triazine-based covalent organic polymer for efficient CO_2 adsorption. Chem Commun 51:10050–10053
31. Sayyah SM, Khaliel AB, Aboud AA, Mohamed SM (2014) Chemical polymerization kinetics of poly-o-phenylenediamine and characterization of the obtained polymer in aqueous hydrochloric acid solution using $K_2Cr_2O_7$ as oxidizing agent. Int J Polym Sci 16:520910
32. Qu F, Yan H, Li K, You J (2020) Han W (2020) A covalent organic framework–MnO_2 nanosheet system for determination of glutathione. J Mater Sci 55:10022–10034
33. Pareek K, Rohana R, Cheng H (2015) Polymeric organo–magnesium complex for room temperature hydrogen physisorption. RSC Adv 5:10886–10891
34. Arul P, John SA (2017) Silver nanoparticles built-in zinc metal organic framework modified electrode for the selective non-enzymatic determination of H_2O_2. Electrochimi Acta 235:680–689
35. Arul P, Narayanamoorthi E, John SA (2020) Covalent organic framework film as an effective electrocatalyst for the simultaneous determination of dihydroxybenzene isomers in water samples. Sens Actuators B Chem 313:128033
36. Ouyang X, Luo L, Ding Y, Liu B, Xu D (2014) Simultaneous determination of purine and pyrimidine bases in DNA using poly(3,4-ethylenedioxythiophene)/graphene composite film. J Electroanal Chem 735:51–56
37. Xu Q, Liu X, Li H, Yin L, Hu X (2013) Electrochemical determination of purine and pyrimidine DNA bases based on the recognition properties of azocalix[4]arene. Biosens Bioelectron 42:355–361
38. Ren S, Wang H, Zhang H, Yu L, Li M, Li M (2015) Direct electrocatalytic and simultaneous determination of purine and pyrimidine DNA bases using novel mesoporous carbon fibers as electrocatalyst. J Electroanal Chem 750:65–73

Publisher's note Springer Nature remains neutral with regard to jurisdictional claims in published maps and institutional affiliations.